

## Mono- and Di-Gold(I) Naphthalenes and Pyrenes: Syntheses, Crystal Structures, and Photophysics

Lei Gao,<sup>†</sup> Miya A. Peay,<sup>†</sup> David V. Partyka,<sup>†</sup> James B. Updegraff III,<sup>†</sup> Thomas S. Teets,<sup>‡</sup> Arthur J. Esswein,<sup>‡</sup> Matthias Zeller,<sup>§</sup> Allen D. Hunter,<sup>§</sup> and Thomas G. Gray<sup>\*,†</sup>

<sup>†</sup>Department of Chemistry, Case Western Reserve University, Cleveland, Ohio 44106.

<sup>‡</sup>Department of Chemistry, Massachusetts Institute of Technology, Cambridge, Massachusetts 02139, and

<sup>§</sup>Department of Chemistry, Youngstown State University, 1 University Plaza, Youngstown, Ohio 44555

Received June 17, 2009

(Phosphine)- and (N-heterocyclic carbene)gold(I) derivatives of naphthalene and pyrene are reported, containing one or two gold atoms per hydrocarbon. The new complexes are prepared by arylation of gold(I) substrates by arylboronic acids or aryl pinacolboronate esters in the presence of cesium carbonate. Isolated yields range from 52% to 98%. The boron precursors themselves derive from the parent hydrocarbon, where boron is installed in an iridium-catalyzed reaction, or from the aromatic bromides, which are borylated with palladium catalysis. Most of the new gold(I) complexes are air- and moisture-stable colorless solids; they are characterized by multinuclear NMR and optical spectroscopy, combustion analysis, and high-resolution mass spectrometry. X-ray diffraction crystal structures are reported for seven. Gold binding red-shifts optical absorption profiles, which are characteristic of the aromatic skeleton. All compounds show triplet-state luminescence, and dual singlet and triplet emission occurs in some instances. Phosphorescence persists for milliseconds at 77 K and for hundreds of microseconds at room temperature. The compounds' photophysical characteristics, along with time-dependent density-functional theory calculations, suggest emission from  $\pi\pi^*$  states of the aromatic core. Triplet-state geometry optimization finds minimal geometric rearrangement upon one-electron promotion from the (singlet) ground state.

### Introduction

The (phosphine)- and (N-heterocyclic carbene)gold(I) fragments are isolobal with the proton;<sup>1,2</sup> they bind terminally to aromatic carbons much like hydrogen and the halogens.<sup>3–7</sup> These gold fragments' identities as relativistic functional

groups are gaining recognition.<sup>8–13</sup> The spin–orbit coupling constant of 5d-electrons in gold is  $5090\text{ cm}^{-1}$ ,<sup>14</sup> that of a 5p-electron in iodine is  $5700\text{ cm}^{-1}$ .<sup>15</sup>

The heavy-atom effect<sup>16–22</sup> of gold ( $Z = 79$ ) influences both ground- and excited-state properties. Gorin and Toste<sup>23</sup> have summarized relativistic effects on homogeneous catalysis with gold. The Lewis acidity of  $\text{LAu}^+$  fragments ( $L = \text{PR}_3$ , N-heterocyclic carbene) is partly ascribable to the relativistic contraction of the gold 6s orbital, which dominates bonding in a two-coordinate linear geometry.<sup>24</sup> The low-energy LUMO of  $\text{LAu}^+$  in turn stabilizes the LUMOs of gold-alkyne complexes and promotes their reactivity toward incoming nucleophiles.

\*To whom correspondence should be addressed. E-mail: tgray@case.edu.

(1) Albright, T. A.; Burdett, J. K.; Whangbo, M.-H. *Orbital Interactions in Chemistry*; Wiley-Interscience: New York, 1985; pp 402–421.

(2) Elian, M.; Chen, M. M. L.; Mingos, D. M. P.; Hoffmann, R. *Inorg. Chem.* **1976**, *15*, 1148–1155.

(3) Schmidbaur, H.; Schier, A. In *Comprehensive Organometallic Chemistry III*; Crabtree, R., Mingos, M., Eds.; Elsevier: 2006; Vol. 2, Section 2.05.

(4) Porter, K. A.; Schier, A.; Schmidbaur, H. *Perspectives in Organometallic Chemistry*; Royal Society of Chemistry, 2003; Vol. 287, pp 74–85.

(5) Fernández, E. J.; Laguna, A.; Olmos, M. E. *Adv. Organomet. Chem.* **2005**, *52*, 77–141.

(6) Schmidbaur, H.; Grohmann, A.; Olmos, M. E. In *Gold: Progress in Chemistry, Biochemistry and Technology*; Schmidbaur, H., Ed.; Wiley: Chichester, 1999.

(7) Schmidbaur, H. Organogold Compounds. In *Gmelin Handbuch der Anorganischen Chemie*, 8th ed.; Slawisch, A., Ed.; Springer-Verlag: Berlin, 1980.

(8) Partyka, D. V.; Zeller, M.; Hunter, A. D.; Gray, T. G. *Angew. Chem., Int. Ed.* **2006**, *45*, 8188–8191.

(9) Gray, T. G. *Comments Inorg. Chem.* **2007**, *28*, 181–212.

(10) Chao, H.-Y.; Lu, W.; Li, Y.; Chan, M. C. W.; Che, C.-M.; Cheung, K.-K.; Zhu, N. J. *Am. Chem. Soc.* **2002**, *124*, 14696–14706.

(11) Jansen, M. *Solid State Sci.* **2005**, *7*, 1464–1474.

(12) Che, C.-M.; Chao, H.-Y.; Miskowski, V. M.; Li, Y.; Cheung, K.-K. *J. Am. Chem. Soc.* **2001**, *123*, 4985–4991.

(13) Kaltsoyannis, N. *J. Chem. Soc., Dalton Trans.* **1997**, 1–11.

(14) Griffith, J. S. *Theory of Transition Metal Ions*; Cambridge University Press: Cambridge, 1964; pp 437–439.

(15) Friedrich, J.; Metz, F.; Dörr, F. *Mol. Phys.* **1975**, *30*, 289–312.

(16) El-Sayed, M. A. *Acc. Chem. Res.* **1968**, *1*, 8–16.

(17) Lower, S. K.; El-Sayed, M. A. *Chem. Rev.* **1966**, *66*, 199–241.

(18) Omary, M. A.; Mohamed, A. A.; Rawashdeh-Omary, M. A.; Fackler, J. P., Jr. *Coord. Chem. Rev.* **2005**, *249*, 1372–1381.

(19) Mohamed, A. A.; Rawashdeh-Omary, M. A.; Omary, M. A.; Fackler, J. P., Jr. *Dalton Trans.* **2005**, 2597–2602.

(20) Omary, M. A.; Rawashdeh-Omary, M. A.; Diyabalanage, H. V. K.; Dias, H. V. R. *Inorg. Chem.* **2003**, *42*, 8612–8614.

(21) Elbjeirami, O.; Burrell, C. N.; Gabbai, F. P.; Omary, M. A. *J. Phys. Chem. C* **2007**, *111*, 9522–9529, and references therein.

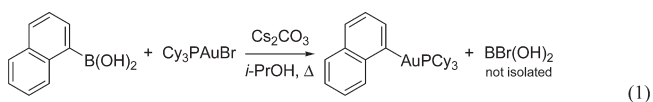
(22) Turro, N. J. *Modern Molecular Photochemistry*; University Science Books: Sausalito, CA, 1991; pp 191–194.

(23) Gorin, D. J.; Toste, F. D. *Nature* **2007**, *446*, 395–403.

(24) Antes, I.; Frenking, G. *Organometallics* **1995**, *14*, 4263–4268.

Relativity alters the optical properties of organogold compounds. Auophilicity, the mutual attraction between gold centers, derives partly from relativity but also from electron correlation.<sup>25,26</sup> Auophilic contacts between gold-(I) sites often produce nonstructured luminescence, especially at low temperatures.

Reports from this laboratory demonstrate that aryl-group transfer from boronic acids or boronate esters attaches aromatic skeletons to gold(I) under mild conditions.<sup>8</sup> Earlier publications by Fackler, Schmidbaur, and their co-workers documented phenyl group transfer to gold(I) from tetraphenylborate anion.<sup>27,28</sup> An example is 1-naphthyl group transfer to a (phosphine)gold(I) bromide, eq 1:



This protocol avoids pyrophoric reagents entirely. Two gold-bearing 1-pyrenyls were prepared from pyrene-1-boronic acid, and a preliminary account of their syntheses and photophysics is available.<sup>29</sup> Subsequent reports of pyrene bearing one or two (Ph<sub>3</sub>P)Au<sup>I</sup> moieties and of (Ph<sub>3</sub>P)Au-(2-naphthyl) have appeared,<sup>30,31</sup> but these compounds are prepared by lithiation of aryl bromide precursors. Access to organogold complexes is limited by the availability of suitable haloaromatic reactants.

The base-supported protocol of eq 1 is simple to execute and accommodates a range of functionalities. Gold(I) aryls bearing nitro, carbonyl, and heterocyclic substituents have all been prepared in good yields.<sup>8</sup> These functional groups are unlikely to survive classical auration reactions, which entail lithiation or magnesiation protocols.

The choice of boron-containing precursors does *not* require lithiation for eventual gold binding. Mild catalytic means affix boronate esters to aromatic molecules. Miyaura and co-workers disclosed the formation of arylpinacolboronate esters from bis(pinacolato)diboron and aryl bromides, iodides,<sup>32</sup> and triflates<sup>33</sup> with (dppf)PdCl<sub>2</sub> (dppf = 1,1'-bis-[diphenylphosphino]ferrocene) in the presence of potassium acetate in polar solvents. Shortly thereafter, Masuda and co-workers<sup>34</sup> reported a similar boronation reaction using pinacolborane as the boron source and amines as supporting bases.<sup>35</sup> Miyaura and collaborators<sup>36</sup> reported reaction conditions that produce arylboronic esters from aryl chlorides and aryl bromides. Fürstner and Seidel have disclosed a

microwave-assisted protocol that transforms aryl chlorides into arylpinacolboronate esters.<sup>37</sup> Recently Buchwald and collaborators have reported efficient palladium-catalyzed borylation reactions of aryl chlorides<sup>38</sup> and aryl (pyrrolyl) bromides.<sup>39</sup> These reactions require a supporting base and are promoted by dialkylbiarylphosphine ligands.

Precursors to boronate esters need not be aryl halides or triflates. Much progress<sup>40,41</sup> has followed from investigations of transition element-catalyzed borylation of arenes. Marder and collaborators have described iridium-catalyzed borylation reactions of naphthalene, pyrene,<sup>42</sup> and other aromatics.<sup>43</sup> These reactions bypass prefunctionalized reagents such as aryl iodides or triflates. They differ in regioselectivity from electrophilic aromatic substitution. For example, pyrene borylates at the 2- and 7-positions in one pot.<sup>42,44</sup> To obtain 2- or 2,7-disubstituted pyrenes requires reduction to a tetrahydropyrene species, followed by electrophilic attack and rearomatization.<sup>45–47</sup> The regioselectivity of iridium-catalyzed borylation possibly derives from an encumbered intermediate, the 16-electron species [Ir(bpy)(Bpin)<sub>3</sub>] (bpy = 2,2'-bipyridine; Bpin = pinacolboronate), which is proposed to undergo a rate-limiting C–H bond activation step.<sup>48</sup> Carbon–hydrogen bonds adjacent to ring junctures or substituents resist borylation.

Thus, palladium- and iridium-catalyzed borylation protocols are complementary. Palladium-catalyzed borylation necessitates halide or sulfonic ester reactants that are accessed by electrophilic aromatic substitution. Iridium-based borylation is dominated by sterics and delivers a different set of functionalized aromatics that classical methods achieve with difficulty. However, they can produce mixtures of products that require nontrivial separation.

Reported here are the syntheses, structures, and optical spectroscopy of new mono- and digold naphthalenes and pyrenes. The use of boron reagents leads to digold aryls that appear inaccessible by lithiation because of competing reduction of gold(I) to the element by dilithioarenes. Emplacement of a single gold atom endows the hydrocarbon skeleton with triplet-state photophysics. In several compounds, both singlet fluorescence and triplet phosphorescence are jointly observable at room temperature. The result is a direct assessment of the energy gap between the first singlet and triplet excited states. Nine new gold(I) compounds are reported, of which seven are crystallographically characterized. Time-dependent density-functional theory calculations find the luminescence to be intraligand in nature. Geometry optimizations of the lowest

(25) Schmidbaur, H.; Schier, A. *Chem. Soc. Rev.* **2008**, *37*, 1931–1951.

(26) Schmidbaur, H. *Chem. Soc. Rev.* **1995**, *24*, 391–400.

(27) Forward, J. M.; Fackler, J. P., Jr.; Staples, R. J. *Organometallics* **1995**, *14*, 4194–4198.

(28) Sladek, A.; Hofreiter, S.; Paul, M.; Schmidbaur, H. *J. Organomet. Chem.* **1995**, *501*, 47–51.

(29) Partyka, D. V.; Esswein, A. J.; Zeller, M.; Hunter, A. D.; Gray, T. G. *Organometallics* **2007**, *26*, 3279–3282.

(30) Heng, W. Y.; Hu, J.; Yip, J. H. K. *Organometallics* **2007**, *26*, 6760–6768.

(31) Osawa, M.; Hoshino, M.; Daisuke, H. *Dalton Trans.* **2008**, 2248–2252.

(32) Ishiyama, T.; Murata, M.; Miyaura, N. *J. Org. Chem.* **1995**, *60*, 7508–7510.

(33) Ishiyama, T.; Itoh, Y.; Kitano, T.; Miyaura, N. *Tetrahedron Lett.* **1997**, *38*, 3447–3450.

(34) Murata, M.; Watanabe, S.; Masuda, Y. *J. Org. Chem.* **1997**, *62*, 6458–6459.

(35) Murata, M.; Oyama, T.; Watanabe, S.; Masuda, Y. *J. Org. Chem.* **2000**, *65*, 164–168.

(36) Ishiyama, T.; Ishida, K.; Miyaura, N. *Tetrahedron* **2001**, *57*, 9813–9816.

(37) Fürstner, A.; Seidel, G. *Org. Lett.* **2002**, *4*, 541–543.

(38) Billingsley, K. L.; Barder, T. E.; Buchwald, S. L. *Angew. Chem., Int. Ed.* **2007**, *46*, 5359–5363.

(39) Billingsley, K. L.; Anderson, K. W.; Buchwald, S. L. *Angew. Chem., Int. Ed.* **2006**, *45*, 3484–3488.

(40) Ishiyama, T.; Miyaura, N. *Chem. Rec.* **2004**, *3*, 271–280.

(41) Ishiyama, T.; Miyaura, N. *J. Organomet. Chem.* **2003**, *680*, 3–11.

(42) Coventry, D. N.; Batsanov, A. S.; Goeta, A. E.; Howard, J. A. K.; Marder, T. B.; Perutz, R. N. *Chem. Commun.* **2005**, 2172–2174.

(43) Mkhali, I. A. I.; Coventry, D. N.; Albesa-Jove, D.; Batsanov, A. S.; Howard, J. A. K.; Perutz, R. N.; Marder, T. B. *Angew. Chem., Int. Ed.* **2006**, *45*, 489–491.

(44) Cho, J.-T.; Tse, M. K.; Holmes, D.; Meleczka, R. E., Jr.; Smith, M. R. III. *Science* **2002**, *295*, 305–308.

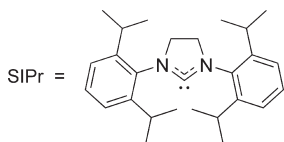
(45) Lee, H.; Harvey, R. G. *J. Org. Chem.* **1986**, *51*, 2847–2848.

(46) Connor, M. D.; Allen, D. S.; Collard, D. M.; Liotta, C. L.; Schiraldi, D. A. *J. Org. Chem.* **1999**, *64*, 6888–6890.

(47) Godinez, C. E.; Zepeda, G.; Garcia-Garibay, M. A. *J. Am. Chem. Soc.* **2002**, *124*, 4701–4707.

(48) Tamura, H.; Yamazaki, H.; Sato, H.; Sakaki, S. *J. Am. Chem. Soc.* **2003**, *125*, 16114–16126.

triplet states are discussed. Comparisons with optimized ground states and crystal structures are made. We demonstrate that (phosphine)- and (N-heterocyclic carbene)gold(I) termini act as relativistic functional groups that transform the photo-physics of hydrocarbon frameworks. Portions of this work have been previously communicated.<sup>8,29</sup>



## Experimental Section

Cy<sub>3</sub>PAuBr and SIPrAuBr were synthesized using methods documented for related phosphine-ligated gold(I) chlorides;<sup>49</sup> Cy<sub>3</sub>PAuN<sub>3</sub> was prepared as previously.<sup>50,51</sup> **Caution:** Metal azide complexes are potentially explosive and precautions are necessary. Cy<sub>3</sub>PAuOAc was prepared analogously to the triphenylphosphine complex.<sup>52</sup> All other solvents and reagents were used as received. Metalation reaction mixtures were stirred vigorously under argon to ensure thorough mixing. Combustion analyses (C, H, and N) were performed by Robertson MicroLIT Laboratories, Madison, NJ. NMR spectra (<sup>1</sup>H, <sup>13</sup>C{<sup>1</sup>H}, and <sup>31</sup>P{<sup>1</sup>H}) were recorded on a Varian AS-400 spectrometer. Chemical shifts are reported in parts-per-million relative to Si(CH<sub>3</sub>)<sub>4</sub> (<sup>1</sup>H, <sup>13</sup>C) or 85% aqueous H<sub>3</sub>PO<sub>4</sub> (<sup>31</sup>P). Mass spectrometry was performed at The Ohio State University and the University of Cincinnati mass spectrometry facilities. Compounds **1**, **13**, and **14** were synthesized following the literature procedures.<sup>42</sup> Compound **4** was purchased from Frontier Scientific, Inc.

**Syntheses of 4,4,5,5-Tetramethyl-2-(2-(4,4,5,5-tetramethyl-1,3,2-dioxaborolan-2-yl)naphthalen-6-yl)-1,3,2-dioxaborolane (2) and 4,4,5,5-Tetramethyl-2-(2-(4,4,5,5-tetramethyl-1,3,2-dioxaborolan-2-yl)naphthalen-7-yl)-1,3,2-dioxaborolane (3).** 2,6-Dibromonaphthalene or 2,7-dibromonaphthalene (122.2 mg, 0.4273 mmol), bis(pinacolato)diboron (227.9 mg, 0.8975 mmol), and potassium acetate (KOAc) (126.4 mg, 1.30 mmol) were mixed in 5 mL of 1,4-dioxane and degassed (solution 1). Pd(dba)<sub>2</sub> (dba = dibenzylideneacetone) (14 mg, 0.024 mmol) and tricyclohexylphosphine (PCy<sub>3</sub>) (16 mg, 0.057 mmol) were mixed in 5 mL of degassed 1,4-dioxane, and the resultant red solution was stirred for 30 min (solution 2). Solution 1 was added to solution 2 with stirring. After 10 min, the mixture was heated to 80 °C for 24 h under an argon atmosphere. During the course of reaction, the reaction mixture took on a pale yellow color and later evolved into a black suspension. After 24 h, 1,4-dioxane was removed by rotary evaporation. The product was extracted into 100 mL of dichloromethane. The yellow dichloromethane solution was then washed with water twice, and the organic layer was collected and dried over MgSO<sub>4</sub>. The solution was then filtered through a layer of silica gel and Celite under vacuum. Solvent was removed and a yellow solid was collected. Sublimation under vacuum at 150–160 °C yielded the analytically pure white product. Yield for **2**: 83.0 mg, 51%. <sup>1</sup>H NMR (CDCl<sub>3</sub>): δ (ppm) 8.41 (s, 2H, naphthyl), 7.83 (dd, 4H, *J* = 5.2 Hz, 8.0 Hz, naphthyl), 1.38 (s, 24H, C(CH<sub>3</sub>)<sub>4</sub>). Yield for **3**: 89.3 mg, 55%. <sup>1</sup>H NMR (CDCl<sub>3</sub>): δ (ppm), 8.35 (s, 2H, naphthyl), 7.83 (dd, 4H, *J* = 6.0 Hz, 8.0 Hz, naphthyl), 1.39 (s, 24H, C(CH<sub>3</sub>)<sub>4</sub>). These compounds were used without further purification.

(49) Schneider, D.; Schier, A.; Schmidbaur, H. *Dalton Trans.* **2004**, 1995–2005.

(50) Partyka, D. V.; Robilotto, T. J.; Zeller, M.; Hunter, A. D.; Gray, T. G. *Proc. Natl. Acad. Sci., U.S.A.* **2008**, *105*, 14293–14297.

(51) Partyka, D. V.; Robilotto, T. J.; Updegraff, J. B. III; Zeller, M.; Hunter, A. D.; Gray, T. G. *Organometallics* **2009**, *28*, 795–801.

(52) Fackler, J. P., Jr.; Khan, M. N. I.; King, C.; Staples, R. J.; Winpenney, R. E. P. *Organometallics* **1991**, *10*, 2178–2183.

**Compound 5:** Cy<sub>3</sub>PAuBr (88 mg, 0.16 mmol), **1** (78.8 mg, 0.31 mmol), and Cs<sub>2</sub>CO<sub>3</sub> (197 mg, 0.60 mmol) were suspended in 10 mL of isopropyl alcohol. After degassing, the reaction vessel was immersed in a 50 °C oil bath and stirred under argon for 24 h. Isopropyl alcohol was removed by rotary evaporation, the remaining solid was extracted into 50 mL of benzene, and the solution was filtered through Celite. Benzene was then removed by rotary evaporation. The residue was washed using hexanes twice and triturated with pentane. After removing pentane by rotary evaporation, a white solid was collected. The white solid was then dissolved in a minimum amount of benzene and filtered through Celite. Crystallization by diffusing pentane into the concentrated benzene solution afforded the product as colorless crystals. Yield: 62 mg, 64%. <sup>1</sup>H NMR (C<sub>6</sub>D<sub>6</sub>): δ (ppm) 8.58 (d, 1H, *J* = 6.0 Hz, 2-naphthyl), 8.28 (dd, 1H, *J* = 8.0 Hz, 4.4 Hz, 2-naphthyl), 7.92 (d, 1H, *J* = 8.0 Hz, 2-naphthyl), 7.86 (d, 1H, *J* = 8.0 Hz, 2-naphthyl), 7.78 (d, 1H, *J* = 8.0 Hz, 2-naphthyl), 7.24–7.36 (m, 2H, 2-naphthyl), 1.39–1.90 (m, 33H, C<sub>6</sub>H<sub>11</sub>). <sup>31</sup>P{<sup>1</sup>H} NMR (C<sub>6</sub>D<sub>6</sub>): δ (ppm) 57.6. HR-MS (ES<sup>+</sup>): calcd *m/z* = 605.2612 (M + H)<sup>+</sup>; found *m/z* = 605.2571. Anal. Calcd for C<sub>28</sub>H<sub>40</sub>AuP: C, 55.63; H, 6.67. Found: C, 55.65; H, 6.82. UV-vis (THF): λ (ε) 279 (5.9 × 10<sup>3</sup> M<sup>-1</sup> cm<sup>-1</sup>), 289 (5.7 × 10<sup>3</sup> M<sup>-1</sup> cm<sup>-1</sup>), 300 (3.8 × 10<sup>3</sup> M<sup>-1</sup> cm<sup>-1</sup>), 325 nm (260 M<sup>-1</sup> cm<sup>-1</sup>). Emission (THF, ex. 279 nm): 355, 480, 516, 553, 600 nm. A 56% yield was obtained when using Cy<sub>3</sub>PAuN<sub>3</sub> as the starting material in an otherwise analogous procedure.

**Compound 6:** Cy<sub>3</sub>PAuBr (176 mg, 0.316 mmol), **2** (66.9 mg, 0.176 mmol), and Cs<sub>2</sub>CO<sub>3</sub> (230 mg, 0.704 mmol) were suspended in 5 mL of isopropyl alcohol. Benzene (5 mL) was added to promote dissolution of the starting materials. After degassing, the reaction vessel was immersed in a 50 °C oil bath and stirred under argon for 24 h. After cooling, the solvents were removed by rotary evaporation, and the remaining solid was extracted into 100 mL of dichloromethane. The extract was filtered through Celite. Dichloromethane was removed by rotary evaporation. The residue was washed twice with hexanes (100 mL) and was then triturated with pentane. An off-white solid was collected upon vacuum filtration removal of pentane. The solid was washed with water and hexanes and dried under vacuum. The solid was then dissolved in a minimum amount of dichloromethane and filtered through Celite. Layering ether onto this dichloromethane solution yielded **6** as colorless crystals. Yield: 156 mg, 90%. <sup>1</sup>H NMR (CDCl<sub>3</sub>): δ (ppm) 7.85 (d, 2H, *J* = 5.6 Hz, naphthyl), 7.63–7.64 (m, 2H, naphthyl), 7.55–7.58 (m, 2H, naphthyl) 1.55–2.10 (m, 66H, (C<sub>6</sub>H<sub>11</sub>)<sub>3</sub>). <sup>31</sup>P{<sup>1</sup>H} NMR (CDCl<sub>3</sub>): δ (ppm) 58.0. HR-MS (ES<sup>+</sup>): calcd *m/z* = 1081.4519 (M + H)<sup>+</sup>; found *m/z* = 1081.4612. Anal. Calcd for C<sub>46</sub>H<sub>72</sub>Au<sub>2</sub>P<sub>2</sub>: C, 51.11; H, 6.71. Found: C, 50.84; H, 6.62. UV-vis (CH<sub>2</sub>Cl<sub>2</sub>): λ (ε) 260 (5.74 × 10<sup>4</sup> M<sup>-1</sup> cm<sup>-1</sup>), 294 (1.30 × 10<sup>4</sup> M<sup>-1</sup> cm<sup>-1</sup>), 304 (1.6 × 10<sup>4</sup> M<sup>-1</sup> cm<sup>-1</sup>), 314 (1.3 × 10<sup>4</sup> M<sup>-1</sup> cm<sup>-1</sup>), 333 nm (1.18 × 10<sup>4</sup> M<sup>-1</sup> cm<sup>-1</sup>). Emission (CH<sub>2</sub>Cl<sub>2</sub>, ex. 314 nm): 404, 490, 525, 565, 610 nm.

**Compound 7:** Cy<sub>3</sub>PAuBr (176 mg, 0.316 mmol), **3** (73 mg, 0.192 mmol), and Cs<sub>2</sub>CO<sub>3</sub> (250 mg, 0.768 mmol) were suspended in 5 mL of isopropyl alcohol. Benzene (5 mL) was added to promote dissolution. After degassing, the reaction vessel was immersed in a 50 °C oil bath and stirred under argon for 24 h. Solvents were removed by rotary evaporation, and the remaining solid was extracted into 100 mL of dichloromethane; the extract was filtered through Celite. Dichloromethane was removed evaporatively. The residue was washed using hexanes and water several times and was triturated with pentane. After removing pentane by rotary evaporation, an off-white solid was collected. The solid was then dissolved in a minimum amount of dichloromethane and filtered through Celite. Layering ether onto this dichloromethane solution yielded **7** as colorless crystals. Yield: 147 mg, 85%. <sup>1</sup>H NMR (CDCl<sub>3</sub>): δ (ppm) 7.87 (d, 2H, *J* = 5.2 Hz, naphthyl), 7.59–7.62 (m, 2H, naphthyl), 7.50–7.52 (m, 2H, naphthyl), 1.56–2.10 (m, 66H, (C<sub>6</sub>H<sub>11</sub>)<sub>3</sub>). <sup>31</sup>P{<sup>1</sup>H} NMR (CDCl<sub>3</sub>): δ (ppm) 58.0. Anal. Calcd for

$C_{46}H_{72}Au_2P_2$ : C, 51.11; H, 6.71. Found: C, 50.98; H, 6.64. UV-vis ( $CH_2Cl_2$ ):  $\lambda$  ( $\epsilon$ ) 260 nm ( $6.98 \times 10^4 M^{-1} cm^{-1}$ ). Emission ( $CH_2Cl_2$ , ex. 307 nm): 373, 490, 524, 560 nm.

**Compound 8:**  $Ph_3PAuBr$  (172 mg, 0.319 mmol), **4** (110 mg, 0.640 mmol), and  $Cs_2CO_3$  (196 mg, 0.602 mmol) were suspended in 10 mL of isopropyl alcohol and charged into a round-bottom flask. After degassing, the reaction vessel was immersed in a 50 °C oil bath and stirred under argon for 24 h. Isopropyl alcohol was removed by rotary evaporation, and the remaining solid was extracted into 50 mL of benzene and filtered through Celite. Benzene was removed by rotary evaporation. The residue was triturated with pentanes; the resulting powder was transferred to a vacuum filtration frit and washed with methanol, water, and pentane, and a white solid was collected. The white solid was then dissolved in a minimum amount of benzene and filtered through Celite. Crystallization by diffusing pentane into the concentrated benzene solution afforded the product as pale yellow crystals. Yield: 109 mg, 58%.  $^1H$  NMR ( $C_6D_6$ ):  $\delta$  (ppm) 8.57 (d, 1H,  $J = 6.0$  Hz, 2-naphthyl), 8.28 (dd, 1H,  $J = 8.0$  Hz, 4.8 Hz, 2-naphthyl), 7.93 (d, 1H,  $J = 8.0$  Hz, 2-naphthyl), 7.87 (d, 1H,  $J = 8.0$  Hz, 2-naphthyl), 7.79 (d, 1H,  $J = 7.6$  Hz, 2-naphthyl), 7.42–7.48 (m, 5H, phenyl), 7.26–7.40 (m, 2H, 2-naphthyl), 6.90–7.00 (m, 10H, phenyl).  $^{31}P\{^1H\}$  NMR ( $C_6D_6$ ):  $\delta$  (ppm) 44.0. HR-MS ( $ES^+$ ): calcd  $m/z = 587.1198 (M + H)^+$ ; found  $m/z = 587.1138$ . Anal. Calcd for  $C_{28}H_{22}AuP$ : C, 57.35; H, 3.78. Found: C, 57.23; H, 3.65. UV-vis (THF):  $\lambda$  ( $\epsilon$ ) 276 ( $8.7 \times 10^3 M^{-1} cm^{-1}$ ), 290 ( $7.6 \times 10^3 M^{-1} cm^{-1}$ ), 300 ( $5.4 \times 10^4 M^{-1} cm^{-1}$ ), 325 nm ( $378 M^{-1} cm^{-1}$ ). Emission (THF, ex. 275 nm): 353, 481, 516, 555, 600 nm.

**Compound 9:**  $Ph_3PAuBr$  (168.7 mg, 0.313 mmol), **2** (65.6 mg, 0.173 mmol), and  $Cs_2CO_3$  (224 mg, 0.687 mmol) were suspended in 10 mL of isopropyl alcohol and charged into a round-bottom flask. Benzene (10 mL) was added to promote solubility. After degassing, the reaction vessel was immersed in a 40 °C oil bath and stirred under argon for 24 h. Solvents were removed by rotary evaporation, and the remaining solid was extracted into 100 mL of dichloromethane and filtered through Celite. Dichloromethane was removed by rotary evaporation. The residue was triturated with pentane and vacuum filtered. After triturating with hexanes twice, a pale yellow solid was collected. The solid was then dissolved in a minimum amount of dichloromethane and filtered through Celite. Crystallization by layering ether onto this dichloromethane solution afforded the product as colorless crystals. Yield: 169.7 mg, 92%.  $^1H$  NMR ( $CDCl_3$ ):  $\delta$  (ppm) 7.97 (d, 2H,  $J = 5.6$  Hz, naphthyl), 7.61–7.69 (m, 16H, aromatic H), 7.44–7.52 (m, 18H, aromatic H).  $^{31}P\{^1H\}$  NMR ( $CDCl_3$ ):  $\delta$  (ppm) 44.4. HR-MS ( $ES^+$ ): calcd  $m/z = 1045.1697 (M + H)^+$ ; found  $m/z = 1045.1682$ . Anal. Calcd for  $C_{46}H_{36}Au_2P_2$ : C, 52.89; H, 3.47. Found: C, 52.53; H, 3.40. UV-vis ( $CH_2Cl_2$ ):  $\lambda$  ( $\epsilon$ ) 261 ( $8.74 \times 10^4 M^{-1} cm^{-1}$ ), 296 ( $2.07 \times 10^4 M^{-1} cm^{-1}$ ), 308 ( $2.88 \times 10^4 M^{-1} cm^{-1}$ ), 320 nm ( $2.47 \times 10^4 M^{-1} cm^{-1}$ ). Emission ( $CH_2Cl_2$ , ex. 326 nm): 344, 490, 524, 565, 614 nm.

**Compound 10:** The same procedure was used as for **9**. Sparkling grayish plates were obtained as the product. Crystallization by diffusing ether into the concentrated benzene solution afforded amber crystals. Yield: 98%.  $^1H$  NMR ( $CDCl_3$ ):  $\delta$  (ppm) 7.98 (d, 2H,  $J = 6.0$  Hz, naphthyl), 7.58–7.69 (m, 16H, aromatic H), 7.44–7.53 (m, 18H, aromatic H).  $^{31}P\{^1H\}$  NMR ( $CDCl_3$ ):  $\delta$  (ppm) 44.4. Anal. Calcd for  $C_{46}H_{36}Au_2P_2$ : C, 52.89; H, 3.47. Found: C, 52.87; H, 3.29. UV-vis ( $CH_2Cl_2$ ):  $\lambda$  ( $\epsilon$ ) 290 nm ( $2.7 \times 10^3 M^{-1} cm^{-1}$ ). Emission ( $CH_2Cl_2$ , ex. 310 nm): 345, 361, 380, 490, 525, 563, 680, 724, 760 nm.

**Compound 11:**  $SIPrAuBr$  (214 mg, 0.320 mmol), **2** (67.3 mg, 0.176 mmol), and  $Cs_2CO_3$  (230 mg, 0.704 mmol) were suspended in 5 mL of isopropyl alcohol. Benzene (5 mL) was added to promote solubility. After degassing, the reaction vessel was heated to 45 °C and stirred under argon for 24 h. Solvents were removed by rotary evaporation, and the remaining solid was extracted into 100 mL of dichloromethane and filtered through Celite. Dichloromethane was removed by rotary evaporation. The residue was washed using hexanes (2  $\times$  100 mL) and was

then triturated with pentane. After removing pentane by rotary evaporation, an off-white solid was collected. This solid was then dissolved in a minimum amount of dichloromethane, and hexanes were layered onto the solution. Slow evaporation gave a precipitate that was the analytically pure product. Yield: 189 mg, 91%.  $^1H$  NMR ( $CDCl_3$ )  $\delta$  (ppm): 7.34 (t, 4H,  $J = 8.0$  Hz, CH aromatic), 7.18 (d, 8H,  $J = 8.0$  Hz), 7.08–7.11 (m, 4H, naphthyl), 6.89 (d, 2H,  $J = 8.0$  Hz, naphthyl), 3.97 (s, 8H,  $CH_2$  imidazole), 3.13 (septet, 8H,  $J = 6.8$  Hz,  $CH(CH_3)_2$ ), 1.44 (d, 24H,  $J = 7.2$  Hz,  $CH(CH_3)_2$ ), 1.32 (d, 24H,  $J = 7.2$  Hz,  $CH(CH_3)_2$ ).  $^{13}C$  NMR ( $CDCl_3$ )  $\delta$  (ppm): 217.19 (s, C carbene), 164.02 (s), 146.69 (s), 138.20 (s), 137.36 (s), 134.80 (s), 132.08 (s), 129.29 (s), 124.18 (s), 123.92 (s), 53.66 (s), 28.96 (s), 25.13 (s), 24.05 (s). HR-MS ( $ES^+$ ): calcd  $m/z = 1303.6100 (M + 2H)^{2+}$ ; found  $m/z = 1301.6012 (M^+)$ , 1302.6067 ( $M + H$ ) $^+$ , 1303.6012 ( $M + 2H$ ) $^{2+}$ . Anal. Calcd for  $C_{64}H_{82}Au_2N_4$ : C, 59.05; H, 6.35; N, 4.30. Found: C, 58.90; H, 5.96; N, 3.99. UV-vis ( $CH_2Cl_2$ ):  $\lambda$  ( $\epsilon$ ) 310 nm ( $1.39 \times 10^4 M^{-1} cm^{-1}$ ). Emission ( $CH_2Cl_2$ , ex. 324 nm): 490, 524, 564, 611 nm.

**Compound 12:**  $SIPrAuOAc$  (103.5 mg, 0.1598 mmol), **3** (36.7 mg, 0.0966 mmol), and  $Cs_2CO_3$  (127 mg, 0.390 mmol) were suspended in 5 mL of isopropyl alcohol and charged into a round-bottom flask. Benzene (5 mL) was added to promote solubility. After degassing, the reaction vessel was immersed in a 45 °C oil bath and stirred under argon for 48 h. Solvents were then removed by rotary evaporation, and the remaining solid was extracted into 50 mL of benzene and filtered through Celite. Benzene was then removed by rotary evaporation. The residue was washed using hexanes twice and triturated with pentane. After removing pentane by rotary evaporation, an off-white solid was collected. Vapor diffusion of ether into a concentrated benzene solution yielded no crystals. Evaporative concentration produced an amber solid that was the analytically pure product. Yield: 66 mg, 63%.  $^1H$  NMR ( $CDCl_3$ ):  $\delta$  (ppm) 7.38 (t, 4H,  $J = 5.6$  Hz, CH aromatic), 7.23 (d, 8H,  $J = 5.6$  Hz, naphthyl), 7.15 (d, 2H,  $J = 8.0$  Hz, naphthyl), 7.09 (s, 2H, naphthyl), 6.83 (d, 2H,  $J = 8.0$  Hz, naphthyl) 3.99 (s, 8H,  $CH_2$  imidazole), 3.16 (septet, 8H,  $J = 6.8$  Hz,  $CH(CH_3)_2$ ), 1.48 (d, 24H,  $J = 7.2$  Hz,  $CH(CH_3)_2$ ), 1.35 (d, 24H,  $J = 7.2$  Hz,  $CH(CH_3)_2$ ).  $^{13}C$  NMR ( $CDCl_3$ ):  $\delta$  (ppm) 217.25 (s, C carbene), 164.93 (s), 146.69 (s), 138.04 (s), 136.70 (s), 134.85 (s), 133.42 (s), 130.44 (s), 129.29 (s), 124.20 (s), 123.88 (s), 53.69 (s), 28.92 (s), 25.10 (s), 24.04 (s). Anal. Calcd for  $C_{64}H_{82}Au_2N_4$ : C, 59.05; H, 6.35; N, 4.30. Found: C, 59.33; H, 6.52; N, 4.22. UV-vis ( $CH_2Cl_2$ ):  $\lambda$  ( $\epsilon$ ) 313 nm ( $6.4 \times 10^4 M^{-1} cm^{-1}$ ). Emission ( $CH_2Cl_2$ , ex. 313 nm): 355, 370, 490, 526, 564, 609 nm.

**Compound 15:** To a 100 mL Schlenk flask, **13** (60.0 mg, 0.183 mmol),  $Cs_2CO_3$  (65.5 mg, 0.201 mmol), and  $Cy_3PAuN_3$  (68.7 mg, 0.13 mmol) were suspended in 8 mL of isopropyl alcohol and degassed. The reaction mixture was then stirred under argon at 50 °C for 24 h. Formation of a white precipitate resulted. Solvent was removed by rotary evaporation, and the resulting white powder was dissolved in dichloromethane (10 mL) and washed three times with  $H_2O$  (10 mL portions). The dichloromethane solution was dried with  $Na_2SO_4$ , and solvent was removed by rotary evaporation. Trituration was performed with pentane, and solvent was removed by rotary evaporation. Colorless crystals were formed from evaporation of an acetone solution. Yield: 46 mg, 52%.  $^1H$  NMR ( $C_6D_6$ ):  $\delta$  (ppm) 8.96 (d, 2H,  $J = 4.8$  Hz, pyrenyl), 8.06 (d, 2H,  $J = 8.8$  Hz, pyrenyl), 7.96 (d, 2H,  $J = 7.6$  Hz, pyrenyl), 7.87 (d, 2H,  $J = 8.8$  Hz, pyrenyl), 7.76 (t, 1H,  $J = 7.2$  Hz, pyrenyl), 1.95–1.05 (m, 33H,  $C_6H_{11}$ ) ppm.  $^{31}P\{^1H\}$  NMR ( $C_6D_6$ ):  $\delta$  (ppm) 57.5. Anal. Calcd for  $C_{34}H_{42}AuP$ : C, 60.17; H, 6.24. Found: C, 59.95; H, 6.48. HR-MS ( $ES^+$ ): calcd  $m/z = 679.2768$ ; found  $m/z = 679.3013 (M)^+$ . UV-vis ( $CH_2Cl_2$ ):  $\lambda$  ( $\epsilon$ ) 264 ( $5.3 \times 10^4 M^{-1} cm^{-1}$ ), 328 ( $2.7 \times 10^4 M^{-1} cm^{-1}$ ), 343 nm ( $3.7 \times 10^4 M^{-1} cm^{-1}$ ). Emission ( $CH_2Cl_2$ , ex. 328 nm): 373, 383, 389, 393, 601 nm.

**Compound 16:** A 100 mL Schlenk flask was charged with  $Cs_2CO_3$  (90.4 mg, 0.277 mmol) in 4 mL of isopropyl alcohol. In a

Table 1. Crystallographic Data for New Compounds Collected at 100 ± 2 K

	5	6·CH <sub>2</sub> Cl <sub>2</sub>	7	9	10	15·C <sub>6</sub> H <sub>5</sub> Me	16·C <sub>6</sub> H <sub>6</sub> ·C <sub>8</sub> H <sub>10</sub>
formula	C <sub>28</sub> H <sub>40</sub> AuP	C <sub>47</sub> H <sub>74</sub> Au <sub>2</sub> Cl <sub>2</sub> P <sub>2</sub>	C <sub>46</sub> H <sub>72</sub> Au <sub>2</sub> P <sub>2</sub>	C <sub>46</sub> H <sub>36</sub> Au <sub>2</sub> P <sub>2</sub>	C <sub>52</sub> H <sub>42</sub> Au <sub>2</sub> P <sub>2</sub>	C <sub>34</sub> H <sub>42</sub> AuP	C <sub>52</sub> H <sub>74</sub> Au <sub>2</sub> P <sub>2</sub>
mol wt	604.54	1165.84	1080.91	1044.62	1122.73	678.61	1155.22
cryst syst	triclinic	triclinic	orthorhombic	monoclinic	triclinic	monoclinic	monoclinic
space group	<i>P</i> $\bar{1}$	<i>P</i> $\bar{1}$	<i>Cmc</i> 2 <sub>1</sub>	<i>P</i> 2 <sub>1</sub> / <i>n</i>	<i>P</i> $\bar{1}$	<i>C</i> 2/ <i>c</i>	<i>P</i> 2 <sub>1</sub> / <i>n</i>
<i>a</i> (Å)	9.093(3)	9.901(2)	21.8915(17)	7.9096(16)	9.3178(8)	25.024(5)	9.5322(9)
<i>b</i> (Å)	10.851(4)	14.031(3)	21.9518(19)	12.458(3)	13.9021(13)	13.5950(19)	16.7591(15)
<i>c</i> (Å)	12.724(4)	18.294(4)	17.8889(15)	18.519(4)	17.961(2)	17.044(2)	17.4417(16)
$\alpha$ (deg)	83.910(4)	94.149(3)	90	90	67.6530(10)	90	90
$\beta$ (deg)	78.774(3)	101.681(3)	90	101.521(2)	89.7330(10)	101.493(2)	94.5900(10)
$\gamma$ (deg)	83.093(4)	107.990(3)	90	90	75.5320(10)	90	90
<i>V</i> (Å <sup>3</sup> )	1218.0(7)	2342.2(9)	8596.6(12)	1788.1(6)	2073.1(4)	5682.1(15)	2777.4(4)
<i>Z</i>	2	2	8	2	2	8	2
index ranges	-11 ≤ <i>h</i> ≤ 11 -14 ≤ <i>k</i> ≤ 13 -16 ≤ <i>l</i> ≤ 16	-13 ≤ <i>h</i> ≤ 13 -18 ≤ <i>k</i> ≤ 18 -24 ≤ <i>l</i> ≤ 24	-24 ≤ <i>h</i> ≤ 29 -29 ≤ <i>k</i> ≤ 20 -19 ≤ <i>l</i> ≤ 23	-10 ≤ <i>h</i> ≤ 9 -15 ≤ <i>k</i> ≤ 15 -23 ≤ <i>l</i> ≤ 23	-11 ≤ <i>h</i> ≤ 11 -17 ≤ <i>k</i> ≤ 17 -22 ≤ <i>l</i> ≤ 23	-32 ≤ <i>h</i> ≤ 32 -17 ≤ <i>k</i> ≤ 17 -22 ≤ <i>l</i> ≤ 22	-12 ≤ <i>h</i> ≤ 11 -21 ≤ <i>k</i> ≤ 21 -22 ≤ <i>l</i> ≤ 22
$\rho_{\text{calc}}$ (Mg/m <sup>3</sup> )	1.648	1.653	1.670	1.940	1.799	1.587	1.601
abs coeff (mm <sup>-1</sup> )	6.118	6.469	6.923	8.319	7.182	5.255	5.374
$\theta$ range (deg)	1.64–27.38	1.15–28.28	2.18–30.52	1.98–26.83	1.23–27.30	1.71–27.50	2.34–26.92
<i>F</i> (000)	604	1156	4288	1000	1084	2720	1348
total no. of rflns	14 172	23 996	23 853	18 684	23 831	33 510	30 206
no. of indep rflns	5209 ( <i>R</i> (int) = 0.0231)	9250 ( <i>R</i> (int) = 0.0309)	7738 ( <i>R</i> (int) = 0.0458)	2808 ( <i>R</i> (int) = 0.0618)	9112 ( <i>R</i> (int) = 0.0224)	6526 ( <i>R</i> (int) = 0.0456)	5929 ( <i>R</i> (int) = 0.0297)
no. of params varied	271	535	628	226	505	325	317
final <i>R</i> indices ( <i>I</i> > 2 $\sigma$ ( <i>I</i> ))	<i>R</i> 1 = 0.0200, <i>wR</i> 2 = 0.0554	<i>R</i> 1 = 0.0545, <i>wR</i> 2 = 0.0833	<i>R</i> 1 = 0.0711, <i>wR</i> 2 = 0.1534	<i>R</i> 1 = 0.0569, <i>wR</i> 2 = 0.1122	<i>R</i> 1 = 0.0223, <i>wR</i> 2 = 0.0734	<i>R</i> 1 = 0.0502, <i>wR</i> 2 = 0.1059	<i>R</i> 1 = 0.0183, <i>wR</i> 2 = 0.0422
<i>R</i> indices (all data)	<i>R</i> 1 = 0.0210, <i>wR</i> 2 = 0.0559	<i>R</i> 1 = 0.0383, <i>wR</i> 2 = 0.0765	<i>R</i> 1 = 0.0597, <i>wR</i> 2 = 0.1465	<i>R</i> 1 = 0.0315, <i>wR</i> 2 = 0.0868	<i>R</i> 1 = 0.0196, <i>wR</i> 2 = 0.0641	<i>R</i> 1 = 0.0732, <i>wR</i> 2 = 0.1187	<i>R</i> 1 = 0.0213, <i>wR</i> 2 = 0.0435
GOF	1.050	1.086	1.048	1.025	1.154	1.058	1.104
largest diff peak and hole (e Å <sup>-3</sup> )	3.108 and -1.403	2.084 and -0.994	6.714 and -1.747	1.039 and -1.907	0.879 and -1.388	2.475 and -1.837	0.816 and -0.935

separate round-bottom flask, **14** (60.0 mg, 0.132 mmol) and Cy<sub>3</sub>PAuOAc (212.6 mg, 0.396 mmol) were dissolved in 8 mL of tetrahydrofuran (THF). After degassing both solutions, the THF solution was cannulated into the Schlenk flask containing the isopropyl alcohol suspension, and the mixture was stirred under argon at 50 °C for 24 h. The white precipitate formed during the course of the reaction was collected by filtration and washed with isopropyl alcohol and THF. Colorless crystals were formed from slow evaporation of a xylene solution. Yield: 118.6 mg, 79%. <sup>1</sup>H NMR (C<sub>6</sub>D<sub>6</sub>):  $\delta$  (ppm) 8.91 (d, 4H, *J* = 4.8 Hz, pyrenyl), 8.08 (s, 4H, pyrenyl), 1.95–1.06 (m, 66H, (C<sub>6</sub>H<sub>11</sub>)<sub>2</sub>). <sup>31</sup>P{<sup>1</sup>H} NMR:  $\delta$  (ppm) 57.5. Anal. Calcd for C<sub>52</sub>H<sub>74</sub>Au<sub>2</sub>P<sub>2</sub>: C, 54.07; H, 6.46. Found: C, 54.05; H, 6.39. MS (ES<sup>+</sup>): calcd *m/z* = 1155.2, found *m/z* = 1155.3 (M + H)<sup>+</sup>. UV–vis (CH<sub>2</sub>Cl<sub>2</sub>):  $\lambda$  (ε) 287 (1.1 × 10<sup>5</sup> M<sup>-1</sup> cm<sup>-1</sup>), 332 (3.7 × 10<sup>4</sup> M<sup>-1</sup> cm<sup>-1</sup>), 348 nm (5.9 × 10<sup>4</sup> M<sup>-1</sup> cm<sup>-1</sup>). Emission (CH<sub>2</sub>Cl<sub>2</sub>, ex. 332 nm): 374, 389, 393, 593 nm.

**Luminescence Measurements.** Steady-state emission spectra were recorded at room temperature on a Cary Eclipse fluorescence spectrophotometer or on an automated Photon Technology International (PTI) QM 4 fluorimeter equipped with a 150 W Xe arc lamp and a Hamamatsu R928 photomultiplier tube. Excitation light was excluded with appropriate glass filters. Sample solutions were added to a quartz EPR tube, freeze pump thaw degassed (four cycles, 1 × 10<sup>-5</sup> Torr), and flame-sealed. Low-temperature emission spectra were recorded in rigid solvent glass at 77 K by immersion of the sealed EPR tubes into a liquid nitrogen-filled dewar. Time-resolved phosphorescence lifetime data were collected on a nanosecond laser system described previously.<sup>53</sup>

(53) Loh, Z.-H.; Miller, S. E.; Chang, C. J.; Carpenter, S. D.; Nocera, D. G. *J. Phys. Chem. A* **2002**, *106*, 11700–11708.

**X-ray Structure Determinations.** Single-crystal X-ray data were collected on a Bruker AXS SMART APEX CCD diffractometer using monochromatic Mo K $\alpha$  radiation with the omega scan technique. The unit cells were determined using SMART<sup>54</sup> and SAINT+.<sup>55</sup> Data collection for all crystals was conducted at 100 K (–173.5 °C). All structures were solved by direct methods and refined by full matrix least-squares against *F*<sup>2</sup> with all reflections using SHELXTL.<sup>56</sup> Refinement of extinction coefficients was found to be insignificant. All non-hydrogen atoms were refined anisotropically. All hydrogen atoms were placed in

(54) Bruker Advanced X-ray Solutions. *SMART for WNT/2000* (Version 5.628); Bruker AXS Inc.: Madison, WI, 1997–2002.

(55) Bruker Advanced X-ray Solutions. *SAINTE* (Version 6.45); Bruker AXS Inc.: Madison, WI, 1997–2003.

(56) Bruker Advanced X-ray Solutions; *SHELXTL* (Version 6.10); Bruker AXS Inc.: Madison, WI, 2000.

(57) Frisch, M. J.; Trucks, G. W.; Schlegel, H. B.; Scuseria, G. E.; Robb, M. A.; Cheeseman, J. R.; Montgomery, J. A., Jr.; Vreven, T.; Kudin, K. N.; Burant, J. C.; Millam, J. M.; Iyengar, S. S.; Tomasi, J.; Barone, V.; Mennucci, B.; Cossi, M.; Scalmani, G.; Rega, N.; Petersson, G. A.; Nakatsuji, H.; Hada, M.; Ehara, M.; Toyota, K.; Fukuda, R.; Hasegawa, J.; Ishida, M.; Nakajima, T.; Honda, Y.; Kitao, O.; Nakai, H.; Klene, M.; Li, X.; Knox, J. E.; Hratchian, H. P.; Cross, J. B.; Bakken, V.; Adamo, C.; Jaramillo, J.; Gomperts, R.; Stratmann, R. E.; Yazyev, O.; Austin, A. J.; Cammi, R.; Pomelli, C.; Ochterski, J. W.; Ayala, P. Y.; Morokuma, K.; Voth, G. A.; Salvador, P.; Dannenberg, J. J.; Zakrzewski, V. G.; Dapprich, S.; Daniels, A. D.; Strain, M. C.; Farkas, O.; Malick, D. K.; Rabuck, A. D.; Raghavachari, K.; Foresman, J. B.; Ortiz, J. V.; Cui, Q.; Baboul, A. G.; Clifford, S.; Cioslowski, J.; Stefanov, B. B.; Liu, G.; Liashenko, A.; Piskorz, P.; Komaromi, I.; Martin, R. L.; Fox, D. J.; Keith, T.; Al-Laham, M. A.; Peng, C. Y.; Nanayakkara, A.; Challacombe, M.; Gill, P. M. W.; Johnson, B.; Chen, W.; Wong, M. W.; Gonzalez, C.; and Pople, J. A. *Gaussian 03, Revision D.01*; Gaussian, Inc.: Wallingford, CT, 2004.

Table 2. Syntheses of New Compounds

Gold(I) Precursor	Arylboron Precursor		Time	Product	Isolated Yield (%)
Cy <sub>3</sub> PAuBr		1	24 h		63% (Br)
Cy <sub>3</sub> PAuN <sub>3</sub>			24 h		56% (N <sub>3</sub> )
Cy <sub>3</sub> PAuBr		2	24 h		90%
Cy <sub>3</sub> PAuBr		3	24 h		85%
Ph <sub>3</sub> PAuBr		4	24 h		58%
Ph <sub>3</sub> PAuBr		2	24 h		92%
Ph <sub>3</sub> PAuBr		3	24 h		98%
SIPrAuBr		2	24 h		91%
SIPrAuOAc		3	48 h		63%
Cy <sub>3</sub> PAuN <sub>3</sub>		13	24 h		52%
Cy <sub>3</sub> PAuOAc		14	24 h		79%
					16

standard calculated positions, and all hydrogen atoms were refined with an isotropic displacement parameter 1.2 times that of the adjacent carbon (1.5 times for methyl hydrogen atoms). Compound **6** crystallized with one molecule of methylene chloride disordered over three sites with occupancy rates of 0.526(3), 0.301(6), and 0.173(6). Its C–Cl distances were restrained to be the same, and the ADPs of the disordered methylene chloride atoms were restrained to be similar (SIMU and DELU commands in SHELXTL). Atoms Cl6

and C48, which overlap significantly, were restrained to be isotropic within a standard deviation of 0.02 Å<sup>2</sup>. Refined crystallographic parameters and residuals for all structures appear in Table 1.

**Computations.** Density-functional theory computations were performed within the Gaussian03 program suite.<sup>57</sup> Computations on singlet structures were spin-restricted; those on triplets were unrestricted. Calculations employed the modified Perdew–Wang exchange functional of Adamo

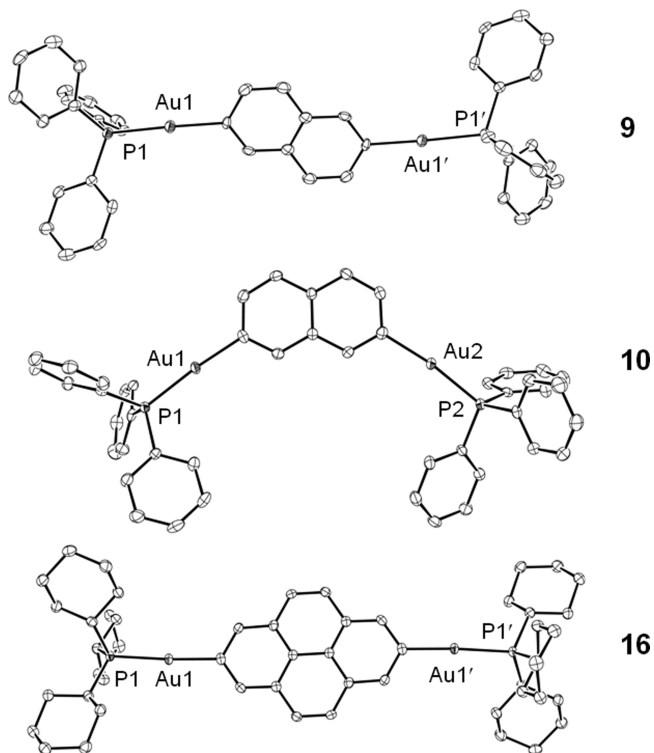
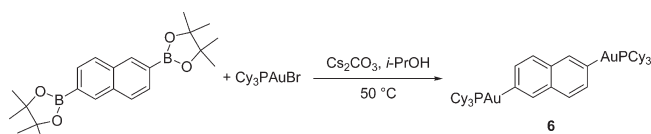


**Figure 1.** Crystal structures (100 K) of new digold(I) organometallics. (a) **9**, (b) **10**, and (c) **16**; 50% probability ellipsoids are shown. Hydrogen atoms and solvent molecules are omitted for clarity. Unlabeled atoms are carbon.

and Barone<sup>58</sup> and the original Perdew–Wang correlation functional.<sup>59</sup> Test calculations performed using other functionals yielded closely similar results. Nonmetal atoms were described with the TZVP basis set of Godbelt, Andzelm, and co-workers.<sup>60</sup> Gold orbitals were described with the Stuttgart effective core potential and the associated basis set,<sup>61</sup> which was contracted as follows: Au, (8s,6p,5d) → [7s,3p,4d]. Relativistic effects with the Stuttgart ECP and its associated basis set are introduced with a potential term (i.e., a one-electron operator) that replaces the two-electron exchange and Coulomb operators resulting from interaction between core electrons and between core and valence electrons. In this way relativistic effects, especially scalar effects, are included implicitly rather than as four-component, one-electron functions in the Dirac equation. Gas-phase equilibrium geometries were optimized in redundant internal coordinates with imposed maximal symmetry for ground-state molecules and without symmetry for excited states. Harmonic frequency calculations verify the resultant structures to be energy minima, except for the ground-state digold model complex **16'**, which exhibits one vibration of frequency 3.81 cm<sup>-1</sup>. Animation of this frequency shows it to be a trimethylphosphine rotor. This imaginary frequency is rectified upon full optimization without symmetry, but the discussion herein derives from the calculation in full C<sub>2h</sub>-symmetry. Investigations in other systems have found changes in optimized geometries upon inclusion of solvent effects to be small,<sup>62</sup> and gas-phase structures are here taken as approximate solution geometries. All other calculated properties reported

(58) Adamo, C.; Barone, V. *J. Chem. Phys.* **1998**, *108*, 664–675.  
 (59) Perdew, J. P.; Wang, Y. *Phys. Rev. B* **1992**, *45*, 13244–13249.  
 (60) Godbout, N.; Salahub, D. R.; Andzelm, J.; Wimmer, E. *Can. J. Chem.* **1992**, *70*, 560–571.  
 (61) Dolg, M.; Wedig, U.; Stoll, H.; Preuss, H. *J. Chem. Phys.* **1987**, *86*, 866–872.  
 (62) Baik, M.-H.; Friesner, R. A. *J. Phys. Chem. A* **2002**, *106*, 7407–7412.

### Scheme 1



here include implicit CH<sub>2</sub>Cl<sub>2</sub> solvation ( $\epsilon = 8.93$ , 298.15 K), which was incorporated in single-point calculations of the gas-phase geometries with Tomasi's polarizable continuum model (PCM).<sup>63,64</sup> Stability tests validated the integrity of all converged densities. Percentage compositions of molecular orbitals, overlap populations, and bond orders between fragments were calculated using the AOMix program of Gorelsky.<sup>65,66</sup> Time-dependent DFT output files were parsed with the program SpectrumWizard, also by Gorelsky.<sup>67</sup>

## Results and Discussion

**Synthesis of Compounds.** Table 2 collects new gold(I) complexes and indicates a numbering scheme. Organogold derivatives of naphthalene and pyrene were prepared from boronated precursors. Scheme 1 depicts a representative synthesis for digold naphthalene derivative **6**. Reactions of boronic acids or pinacolboronate esters of aromatic hydrocarbons with (phosphine)- or (N-heterocyclic carbene)gold(I) complexes in the presence of cesium carbonate in alcohol solvents yield the corresponding arylgold derivatives. The reaction cleaves a carbon–boron bond to form carbon–gold bonds. The use of boron-based reagents avoids stridently reducing conditions incompatible with gold(I) or with sensitive organic functionalities. In our hands, attempts to produce digold complexes from dithionaphthalene afforded elemental gold with no evidence of the desired organometallic products. The gold(I) reactants of choice for binding to aryl skeletons are the (phosphine)- or (N-heterocyclic carbene)gold(I) bromides. Arylation reactions proceed for gold(I) acetates or azide complexes, but lower yields are often recovered. In no case is there evidence for the formation of isomers that would diminish regioselectivity.

Given a choice of arylboronic acid or pinacolboronate ester starting material, the ester is preferable. Residual, unreacted boron reagents typically contaminate crude products. The boronic acid can be washed away with methanol, but the organogold species are partly soluble in this solvent, and their isolated yields suffer. Unreacted pinacolboronate esters are hexanes-soluble, but the gold products are not. The final gold complexes are purified by washing in air without loss of yield. If the gold(I) starting material is in excess, then its surplus contaminates the organometallic product and is difficult to remove with common solvents. Mohr and co-workers have applied this boron-based protocol to the synthesis of a peri-diaurated naphthalene.<sup>68</sup>

(63) Miertus, S.; Scrocco, E.; Tomasi, J. *Chem. Phys.* **1981**, *55*, 117–129.

(64) Tomasi, J.; Mennucci, B.; Cammi, R. *Chem. Rev.* **2005**, *105*, 2999–3093.

(65) Gorelsky, S. I. *AOMix: Program for Molecular Orbital Analysis*; York University: Toronto, 1997, <http://www.sg-chem.net>.

(66) Gorelsky, S. I.; Lever, A. B. P. *J. Organomet. Chem.* **2001**, *635*, 187–196.

(67) Gorelsky, S. I.; *Swizard program, revision 4.5*, <http://www.sg-chem.net/>.

(68) Meyer, N.; Lehmann, C. W.; Lee, T. K.-M.; Rust, J.; Yam, V. W.-W.; Mohr, F. *Organometallics* **2009**, *28*, 2931–2934.

**Table 3.** Selected Interatomic Distances (Å) and Angles (deg) for Aurated Naphthalenes (5–7, 9, 10) and Pyrenes (15 and 16)

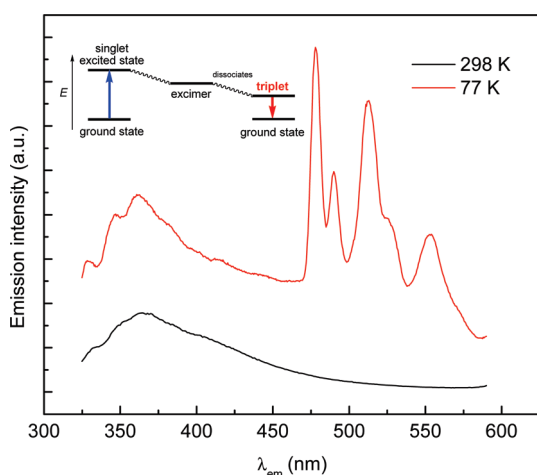
	5	6	7	9	10	15	16
C–Au	2.038(3)	2.035(5) 2.044(5)	2.026(19) 2.00(2) 2.050(12)	2.023(5)	2.051(4), 2.036(3)	2.046(7)	2.046(2)
Au–P	2.2922(9)	2.2984(14) 2.2968(14)	2.303(4) 2.276(5)	2.2643(16)	2.2874(9), 2.2930(9)	2.300(2)	2.3044(6)
∠C–Au–P	177.04(7)	178.75(16) 179.08(15)	178.7(5) 176.0(6) 177.4(5)	175.78(17)	172.04(10), 174.95(10)	173.6(2)	176.09(7)

**Table 4.** <sup>31</sup>P NMR Chemical Shifts Relative to 85% H<sub>3</sub>PO<sub>4</sub>(aq) of Phosphine-Ligated Gold Complexes

complex	solvent	<sup>31</sup> P δ (ppm)	starting material
5	C <sub>6</sub> D <sub>6</sub>	57.6	PCy <sub>3</sub> AuBr (55.5) PCy <sub>3</sub> AuOAc (47.9) PCy <sub>3</sub> AuN <sub>3</sub> (53.9)
6	CDCl <sub>3</sub>	58.0	PCy <sub>3</sub> AuBr (55.5)
7	CDCl <sub>3</sub>	58.0	PCy <sub>3</sub> AuBr (55.5)
8	C <sub>6</sub> D <sub>6</sub>	44.0	PPh <sub>3</sub> AuBr (35.2)
9	CDCl <sub>3</sub>	44.4	PPh <sub>3</sub> AuBr (35.2)
10	CDCl <sub>3</sub>	44.4	PPh <sub>3</sub> AuBr (35.2)
15	C <sub>6</sub> D <sub>6</sub>	57.5	PCy <sub>3</sub> AuN <sub>3</sub> (53.9)
16	C <sub>6</sub> D <sub>6</sub>	57.5	PCy <sub>3</sub> AuOAc (47.9)

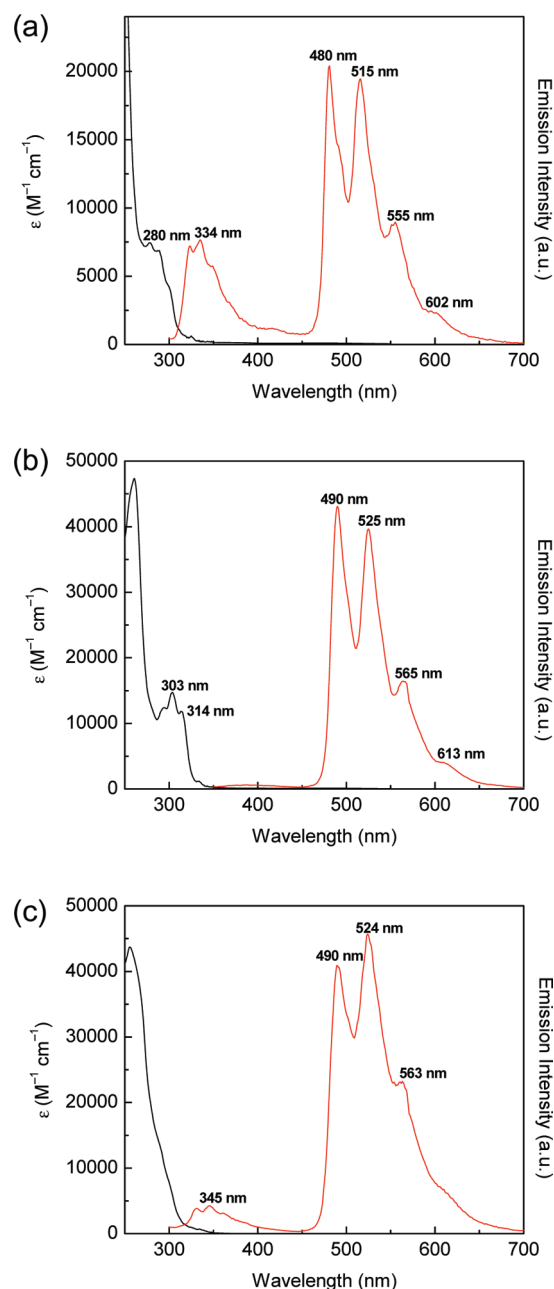
**Table 5.** <sup>13</sup>C Chemical Shifts of Ligand Carbene Carbons Relative to Tetramethylsilane in NHC-Ligated Gold Complexes

complex	<sup>13</sup> C solvent	<sup>13</sup> C δ (ppm) (carbene C)	starting material
11	CDCl <sub>3</sub>	217.2	SIPrAuBr (199.0), SIPrAuN <sub>3</sub> (194.7)
12	CDCl <sub>3</sub>	217.2	SIPrAuOAc (195.5)

**Figure 2.** Emission spectra of (tricyclohexylphosphine)gold(I) 1-naphthyl **17** at 295 K (black) and 77 K (red) in 2-methyltetrahydrofuran glass at  $5 \times 10^{-6}$  M concentration. Inset: a model<sup>29</sup> for the concentration dependence (see text) of triplet-state emission.

The organogold naphthalenes were isolated by extraction into benzene (monogold complexes) or dichloromethane (digold complexes). Solvents were removed *in vacuo*, and the residues were triturated with pentane or hexanes. The products were collected by vacuum filtration and purified by crystallization. The monogold(I) pyrenyl complex **15** was isolated by extraction into dichloromethane. Digold pyrene derivative **16** was collected by filtration.

**Crystal Structures.** Single-crystal X-ray structures of seven new gold complexes have been obtained: five of aurated

**Figure 3.** Absorption (black) and room-temperature emission (red) of (a) monogold **5**, (b) C<sub>2h</sub>-symmetric digold **6**, and (c) C<sub>2v</sub>-symmetric digold **7** in CH<sub>2</sub>Cl<sub>2</sub>.

naphthalenes and two of aurated pyrenes. The crystal structure of **8** has been reported previously.<sup>69</sup> Figure 1 depicts

(69) Osawa, M.; Hoshino, M.; Hashizume, D. *Dalton Trans.* **2008**, 2248–2252.

Table 6. Luminescence Parameters of Gold-Substituted Naphthalenes

compound	solvent	<i>T</i> (K)	<i>E</i> <sub>max</sub> (nm)	λ <sub>em</sub> (nm) <sup>a</sup>	τ (ms)	φ <sub>em</sub>	<i>k</i> <sub>r</sub> × 10 <sup>2</sup> (s <sup>-1</sup> )	<i>k</i> <sub>nr</sub> × 10 <sup>3</sup> (s <sup>-1</sup> )
5	2-MeTHF	295	479	480	0.097	0.0061	0.63	10.24
5	2-MeTHF	77		480	1.72			
5	2-MeTHF	77		605	1.72			
6	1:1 2-MeTHF/CH <sub>2</sub> Cl <sub>2</sub>	295	489	480	0.200	0.022	1.08	4.89
6	1:1 2-MeTHF/CH <sub>2</sub> Cl <sub>2</sub>	77		485	0.541			
6	1:1 2-MeTHF/CH <sub>2</sub> Cl <sub>2</sub>	77		605	0.48			
7	1:1 2-MeTHF/CH <sub>2</sub> Cl <sub>2</sub>	295	490	480	0.220	0.014	0.64	4.48
7	1:1 2-MeTHF/CH <sub>2</sub> Cl <sub>2</sub>	77		480	1.59			
8	2-MeTHF	295	479	480	0.108	0.012	1.07	9.15
8	2-MeTHF	77		480	1.65			
8	2-MeTHF	77		605	1.5			
9	1:1 2-MeTHF/CH <sub>2</sub> Cl <sub>2</sub>	295	490	480	0.210	0.025	1.17	4.64
9	1:1 2-MeTHF/CH <sub>2</sub> Cl <sub>2</sub>	77		480	0.525			
9	1:1 2-MeTHF/CH <sub>2</sub> Cl <sub>2</sub>	77		605	0.48			
10	2-MeTHF	295	491	480	0.20	0.013	0.64	4.94
10	2-MeTHF	77		485	1.53			
10	2-MeTHF	77		605	1.36			
11	1:1 2-MeTHF/CH <sub>2</sub> Cl <sub>2</sub>	295	490	490	0.26	0.032	1.21	3.72
11	1:1 2-MeTHF/CH <sub>2</sub> Cl <sub>2</sub>	77		485	0.494			
11	1:1 2-MeTHF/CH <sub>2</sub> Cl <sub>2</sub>	77		605	0.46			
12	2-MeTHF	295	490	490	0.32	0.014	0.45	3.08
12	2-MeTHF	77		485	1.28			
12	2-MeTHF	77		605	1.17			

<sup>a</sup>Wavelength at which emission lifetime data were collected.

thermal ellipsoid projections of three representative organometallics: two isomeric digold(I) naphthalenes and a digold(I) pyrene. Table 3 reports selected interatomic distances and angles. The asymmetric unit of **6** contains two half-molecules situated on special positions. In the asymmetric unit of **7**, one complete molecule resides on a general position, and one half-molecule on a mirror plane. In the asymmetric unit of **9**, one half-molecule resides on a crystallographic inversion center. Digold pyrene derivative **16** resides on an inversion center such that half the molecule constitutes the asymmetric unit. Gold–carbon bond lengths range from 2.00(2) Å for one independent C–Au bond of **7** to 2.051(4) Å for an independent bond in **10**. Phosphorus–gold bonds range in length from 2.2643(16) Å for **9** to 2.3044(6) Å for **16**. These ranges of gold–(I)–element bond lengths are normal.<sup>70–72</sup> Coordination geometries about gold are essentially linear: C–Au–P bond angles range from 172.04(10)° (one such angle in **10**) to 179.08(15)° (one independent molecule of **6**).

**NMR Spectroscopy.** Multinuclear NMR spectroscopy is diagnostic of product formation. Table 4 collects <sup>31</sup>P chemical shifts, relative to 85% phosphoric acid, for phosphine-ligated organometallics. In contrast to an earlier observation,<sup>30</sup> we do not encounter long-range <sup>31</sup>P–<sup>1</sup>H coupling. Carbene–carbon resonances for N-heterocyclic carbene complexes appear in Table 5. These tables also indicate starting gold(I) reagents and pertinent chemical shifts in the same solvents. Most digold complexes here are insoluble in benzene but dissolve readily in dichloromethane and chloroform, and hence the choice of NMR solvent. Upon carbon–gold bond formation, <sup>31</sup>P resonances of phosphine ligands and carbene–carbon <sup>13</sup>C resonances shift downfield, reflecting the lesser electronegativity of carbon compared to the *trans*-situated donor atoms in the gold reactants and

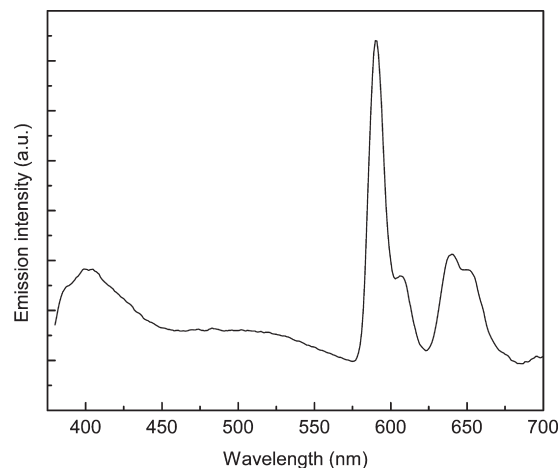


Figure 4. Emission spectrum (77 K) of digold pyrene derivative **16** in a 2-methyltetrahydrofuran glass.

possibly also the *trans*-influence of aryl ligands. In all cases, the shift suffices to distinguish product from gold(I) reactant.

**Optical Spectroscopy.** The new organometallics luminesce in organic solvents. For the gold(I) naphthyl complexes, oxygen-quenchable, structured emission spans wavelengths extending from ca. 475 to 650 nm. This emission onset represents a Stokes shift of some 145 nm (9250 cm<sup>-1</sup>) from the onset of absorption. For complexes having the same number of gold atoms, peak emission wavelengths are somewhat insensitive to gold substitution about the naphthalene core.

The gross temperature-sensitivity of emission is that commonly seen for phosphorescent molecules. An example is the previously reported<sup>8</sup> (tricyclohexylphosphine)-gold(I) 1-naphthyl **17**. At low concentrations of **17**, triplet emission activates only with cooling. Figure 2 depicts luminescence spectra collected in degassed 2-methyltetrahydrofuran at 77 and 295 K. At room temperature, unstructured ultraviolet emission appears; this luminescence is unaltered by exposure to oxygen. At liquid nitrogen temperature, the same luminescence reappears with ingrowing vibronic structure. Near

(70) Partyka, D. V.; Updegraff, J. B., III; Zeller, M.; Hunter, A. D.; Gray, T. G. *Organometallics* **2007**, *26*, 183–186.

(71) Porter, K. A.; Schier, A.; Schmidbaur, H. *Organometallics* **2003**, *22*, 4922–4927.

(72) Fernández, E. J.; Laguna, A.; Olmos, M. E. *Coord. Chem. Rev.* **2008**, *252*, 1630–1667.

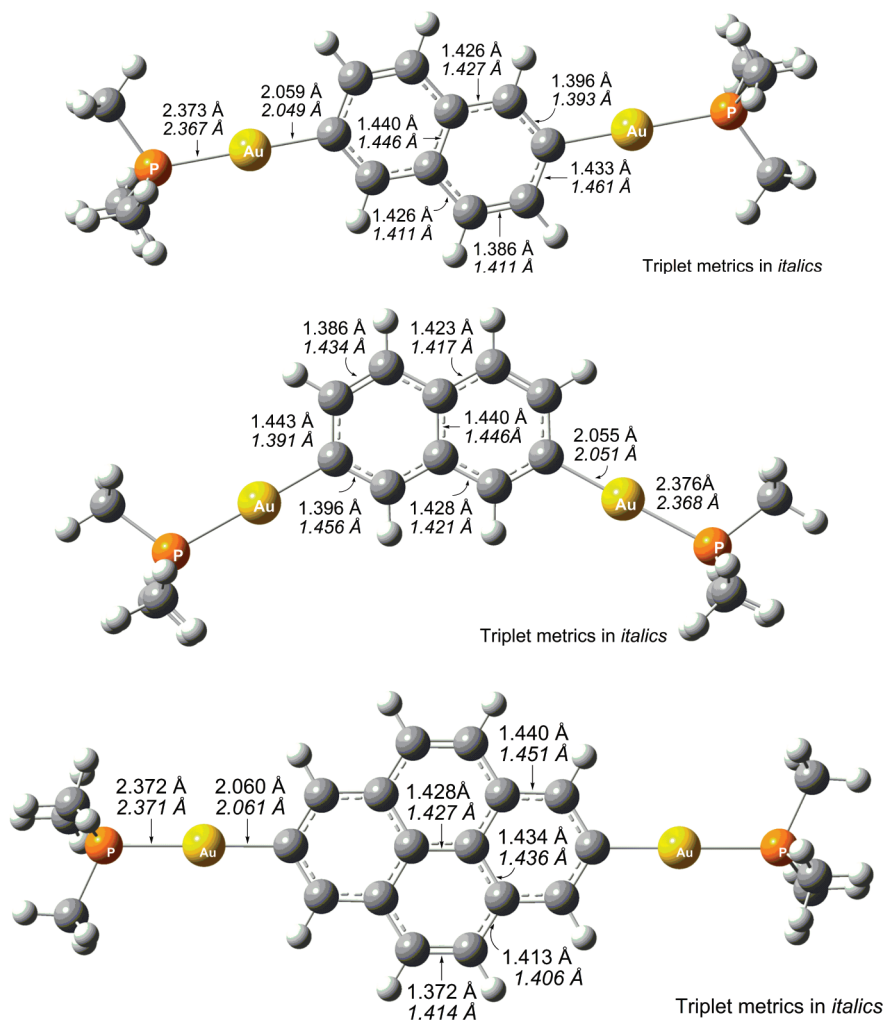


**Figure 5.** Optimized interatomic distances of model digold(I) naphthalene and pyrene derivatives. Top: **6'**. Center: **7'**. Bottom: **16'**. Bond lengths are calculated for the singlet ground state; triplet excited-state distances appear in italics.

475 nm, sharply structured emission appears. This emission is too long-lived (1–2 s) for lifetime measurement on the nanosecond laser available to us; the laser repetition rate is faster than emission decay. At higher concentrations ( $\sim 10^{-4}$  M), this emission occurs at room temperature and is oxygen-quenched. This concentration dependence has been encountered previously, with gold(I)-substituted 1-pyrenyls.<sup>73</sup> The inset of Figure 2 summarizes the proposed mechanism. A nonemissive excimer lies above the triplet state in energy. This excimer catalyzes, or pumps, the formation of the triplet, which then emits long-lifetime, structured luminescence.

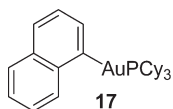


Figure 3 depicts room-temperature absorption and emission spectra of the new monogold 2-naphthyl complex **5** and of the isomeric digold naphthalenes **6** and **7** in dichloromethane. Arene-centered absorptions set in near 330 nm for gold(I) naphthalene complexes; absorption features differ

according to the substitution pattern of the aromatic skeleton. Monogold **5** shows dual luminescence. Structured emission rises near 310 nm and maximizes at 334 nm. An approximate mirror-image relationship exists between it and the absorption feature at 280 nm. The small Stokes shift ( $5700\text{ cm}^{-1}$ ) suggests fluorescence from a singlet excited state. A similar emission is less prominent for  $C_{2v}$ -symmetric digold complex **7**.

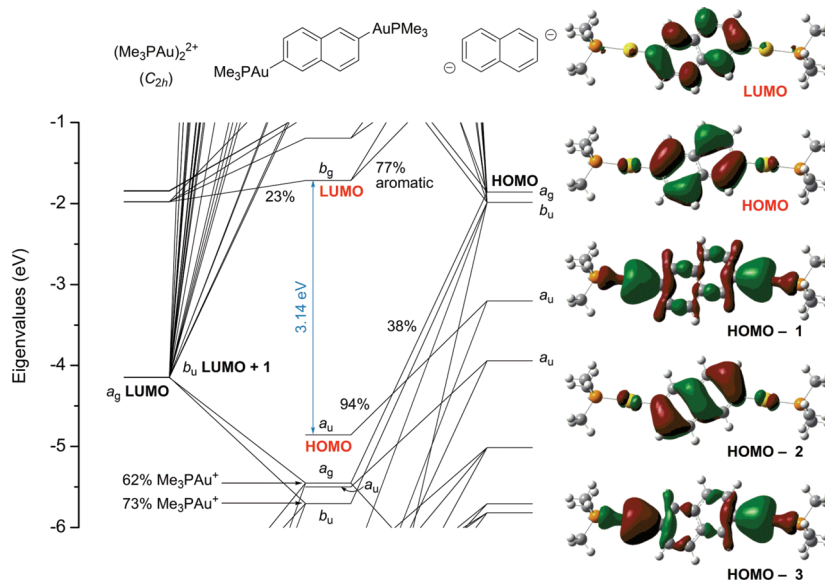
For all three complexes, sharply structured emission sets in near 470 nm. At least three vibronic peaks are clearly resolved with spacings that average  $1425\text{ cm}^{-1}$  for **5**,  $1365\text{ cm}^{-1}$  for **6**, and  $1323\text{ cm}^{-1}$  for **7**. These values concur roughly with tabulated ring-stretching frequencies of aromatic molecules, indicating a vibronic origin for the spiked structure of the 475–650 nm emission profile.<sup>74</sup>

Table 6 summarizes luminescence lifetimes of organogold(I) naphthalenes; these are microsecond-scale or longer at 77 and 295 K. The lifetimes, along with the oxygen-quenching of the emission and the large Stokes shifts, indicate triplet luminescence. The small range of emission maxima complicates standard energy-gap law analyses.<sup>75</sup> The orbital

(74) Pretsch, E.; Bühlmann, P.; Affolter, C. *Structure Determination of Organic Compounds*; Springer: New York, 2000; p 255.

(75) Caspar, J. V.; Kober, E. M.; Sullivan, B. P.; Meyer, T. J. *J. Am. Chem. Soc.* **1982**, *104*, 630–632.

(73) Partyka, D. V.; Esswein, A. J.; Zeller, M.; Hunter, A. D.; Gray, T. G. *Organometallics* **2007**, *26*, 3279–3282.



**Figure 6.** Kohn–Sham orbital energy level diagram of **6'** (mpmpw91/Stuttgart ECP and basis on Au); implicit  $\text{CH}_2\text{Cl}_2$  solvation is included through a continuum dielectric model. (Right) Plots of selected orbitals (contour level 0.03 au). Percentage contributions of (phosphine)gold(I) cation and naphthalene-diyl anion fragments are indicated.

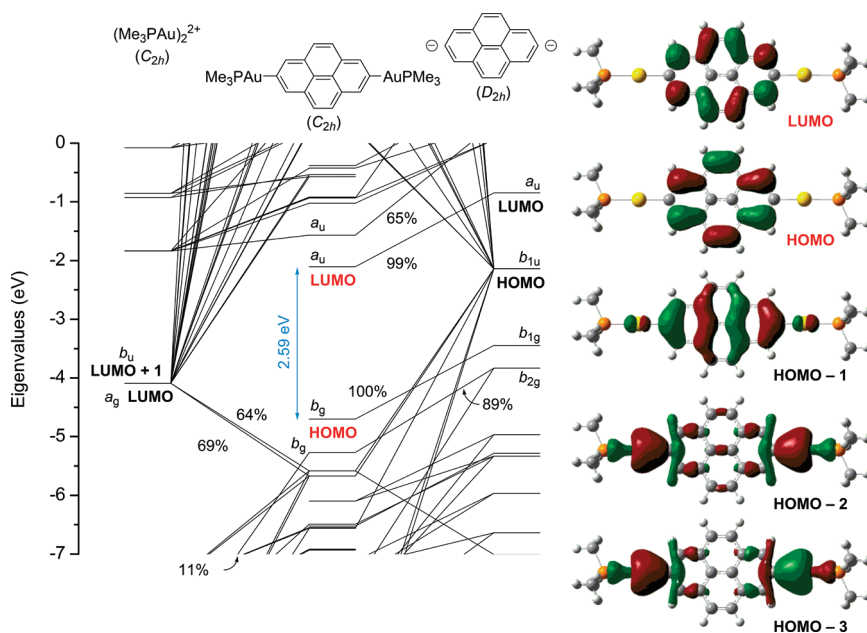


**Figure 7.** Kohn–Sham orbital energy level diagram of aurated pyrene **16'** (mpmpw91/Stuttgart ECP and basis on Au); implicit  $\text{CH}_2\text{Cl}_2$  solvation is included through a continuum dielectric model. (Right) Plots of selected orbitals (contour level 0.03 au). Percentage contributions of (phosphine)gold(I) cation and pyrene-diyl anion fragments are indicated.

percentage of the emitting states and their structures have been examined with quantum chemical computations.

Gold(I) pyrene derivatives are also luminescent, as has been noted previously for complexes isomeric with those reported here.<sup>29,30</sup> Figure 4 reproduces the emission spectrum of digold complex **16** at 77 K in 2-methyltetrahydrofuran glass. Emission is sharply structured with maxima at 591 and 640 nm. The 77 K lifetime of emission collected at 600 nm is 13  $\mu\text{s}$ . We assign the red emission near 600 nm as a triplet-state  $\pi\pi^*$  transition, and the higher-energy luminescence as intraligand fluorescence. Such assignments concur with earlier work<sup>8,29,30</sup> and with time-dependent density-functional theory calculations.

**Calculations.** Density-functional theory (DFT) and time-dependent DFT calculations were performed on model digold(I) complexes. Capping trimethylphosphine ligands replace tricyclohexylphosphine or N-heterocyclic carbenes for computational tractability. Geometry optimizations proceeded with imposed symmetry. Figure 5 collects calculated metrics involving gold for models **6'**, **7'**, and **16'**. These are in good agreement with the crystallographic metrics of Table 3. Gold-donor atom bond lengths are consistently overestimated by ca. 0.02 Å for Au–C and 0.08 Å for Au–P bonds. This behavior is commonly noted for DFT, and comparative studies of optimized structures for a range of common functionals find similar mean

absolute errors in bond lengths.<sup>76,77</sup> The optimized parameters are similar to those stated elsewhere for (phosphine)gold(I) and organogold(I) complexes.<sup>78–84</sup>

Figure 6 depicts a frontier-orbital energy level diagram for digold model complex **6'** in  $C_{2h}$  symmetry. Plots of selected orbitals appear at right. Percentage contributions indicated in the figure are of the total electron density and are calculated from Mulliken population analysis.<sup>85</sup> The corresponding diagram for the non-centrosymmetric digold complex **7'** appears as Figure S5 in the Supporting Information.

The highest occupied Kohn–Sham orbital (HOMO) of **6'** derives (94%) from the naphthalenediyl HOMO–3, which is a  $\pi$ -combination. The lowest unoccupied Kohn–Sham orbital (LUMO) also has preponderant aromatic character (78%), but with a higher contribution from the two (phosphine)gold(I) fragments. The calculated HOMO–LUMO gap is 3.14 eV; that of  $C_{2v}$  isomer **7'** is 3.18 eV, and of 2-naphthyl **5'**, 3.28 eV. Two occupied orbitals, the HOMO–1 and the HOMO–3, account for the two gold–carbon  $\sigma$ -bonds. These are an in-phase and antiphase contribution, respectively. The in-phase combination is the less stable of the pair because more nodal surfaces transect the aromatic bridge in it than in the antiphase HOMO–3. The first several vacant orbitals in the complex have negligible contributions from the (phosphine)gold(I) fragment LUMOs or from occupied gold orbitals. Broadly similar observations pertain to the frontier orbitals of **5'** and **7'**.

Figure 7 depicts an energy-level diagram for the model digold pyrene **16'** with orbital plots at right. This complex is a potential-energy minimum with  $C_{2h}$  symmetry. As with the metalated naphthalenes, its frontier orbitals are  $\pi$ -functions of the pyrenediyl bridging ligand. The HOMO–2 and HOMO–3 compose the two C–Au  $\sigma$ -bonding combinations, with the in-phase orbital again having higher energy. The calculated HOMO–LUMO of **16'** energy levels is 2.59 eV; that of monogold pyrene **15'** is 2.60 eV. The Kohn–Sham orbital energy-level diagrams suggest that low-lying excited states of aurated naphthalenes and pyrenes possess predominant  $\pi$ -character.

Time-dependent DFT calculations find the first several optically allowed transitions to be localized on the aromatic ligands, for the metalated naphthalenes and pyrenes considered here. Table 7 assembles computed singlet–singlet transitions for metalated naphthalenes **6'**, **7'**, and **16'**. Calculated excitations are typically combinations of one-electron promotions that undergo configuration interaction. Those transitions having the greatest oscillator strength are typically

**Table 7. Calculated Excitation Wavelengths, Oscillator Strengths  $f$ , and Principal Orbital Compositions of the Singlet Excited States of Model Complexes **6'**, **7'**, and **16'** Lying beyond 300 nm (dichloromethane solvent)**

Compound <b>6'</b>			
no.	$E$ (nm)	$f$	orbital origin (percentage contribution)
1	347.7	0.2602	HOMO $\rightarrow$ LUMO (67%) HOMO $\rightarrow$ LUMO+1 (18%)
2	327.1	0	HOMO–1 $\rightarrow$ LUMO (97%)
3	325.8	0.0245	HOMO $\rightarrow$ LUMO+1 (44%) HOMO–2 $\rightarrow$ LUMO (39%) HOMO $\rightarrow$ LUMO (11%)
4	309.7	0	HOMO $\rightarrow$ LUMO+3 (100%)
5	309.7	0.0006	HOMO $\rightarrow$ LUMO+4 (100%)
6	308.1	0	HOMO $\rightarrow$ LUMO+2 (96%)
7	306.3	0.0081	HOMO–3 $\rightarrow$ LUMO (96%)
Compound <b>7'</b>			
no.	$E$ (nm)	$f$	orbital origin (percentage contribution)
1	336.2	0.0094	HOMO $\rightarrow$ LUMO (78%) HOMO $\rightarrow$ LUMO+4 (7%)
2	334.9	0.0468	HOMO $\rightarrow$ LUMO+1 (73%) HOMO–2 $\rightarrow$ LUMO (25%)
3	328.6	0.0039	HOMO–1 $\rightarrow$ LUMO (98%)
4	311.4	0	HOMO $\rightarrow$ LUMO+2 (100%)
5	309.0	0.0007	HOMO $\rightarrow$ LUMO+3 (100%)
6	306.3	0	HOMO–3 $\rightarrow$ LUMO (92%) HOMO–1 $\rightarrow$ LUMO+1 (7%)
Compound <b>16'</b>			
no.	$E$ (nm)	$f$	orbital origin (percentage contribution)
1	390.3	0.0002	HOMO $\rightarrow$ LUMO+1 (62%) HOMO–1 $\rightarrow$ LUMO (37%)
2	381.3	0.3928	HOMO $\rightarrow$ LUMO (72%) HOMO–1 $\rightarrow$ LUMO+1 (8%)
3	356.4	0	HOMO–2 $\rightarrow$ LUMO (100%)
4	347.6	0	HOMO–3 $\rightarrow$ LUMO (100%)
5	335.8	0.1394	HOMO–1 $\rightarrow$ LUMO (47%) HOMO $\rightarrow$ LUMO+1 (27%) HOMO $\rightarrow$ LUMO+8 (11%)
6	330.4	0	HOMO $\rightarrow$ LUMO+2 (86%) HOMO–4 $\rightarrow$ LUMO (10%)
7	326.8	0.0006	HOMO $\rightarrow$ LUMO+4 (100%)
8	326.2	0	HOMO $\rightarrow$ LUMO+5 (100%)
9	324.2	0	HOMO $\rightarrow$ LUMO+3 (93%)
10	307.3	1.6964	HOMO–1 $\rightarrow$ LUMO+1 (80%) HOMO–1 $\rightarrow$ LUMO+8 (9%)
11	302.3	0.0106	HOMO–2 $\rightarrow$ LUMO+1 (96%)

delocalized over the aromatic bridge. Where not fully prohibited by symmetry, C–Au  $\sigma$ -to-aryl  $\pi^*$ -transitions have slight oscillator strengths ( $f < 0.03$ ). The metalated arenes calculated here have aryl  $\pi^*$ -functions as their HOMOs and LUMOs, and their low-lying excited states can be assigned as ligand-centered  $\pi$ -states.

Triplet-state structures have been optimized for mono- and digold aromatics. All open-shell calculations were spin-unrestricted. Vibrational analysis finds normal-mode frequencies to be all real numbers, confirming the triplet-state structures to be minima on the (excited-state) energy hypersurface.

Figure 5 assembles calculated metrics of (ground-state) singlet and lowest triplet **6'**, **7'**, and **16'**. Metric changes upon excitation are miniscule; the calculated singlet and triplet geometries are nearer each other than any is to the crystal structures of the respective digold complexes. Both bond

(76) Scheiner, A. C.; Baker, J.; Andzelm, J. W. *J. Comput. Chem.* **1997**, *18*, 775–795.

(77) Elbjerrami, O.; Gonser, M. W. A.; Stewart, B. N.; Bruce, A. E.; Bruce, M. R. M.; Cundari, T. R.; Omary, M. A. *Dalton Trans.* **2009**, 1522–1533.

(78) Bardají, M.; Calhorda, M. J.; Costa, P. J.; Jones, P. G.; Laguna, A.; Pérez, M. R.; Villacampa, M. D. *Inorg. Chem.* **2006**, *45*, 1059–1068.

(79) Hu, X.; Castro-Rodríguez, I.; Olsen, K.; Meyer, K. *Organometallics* **2004**, *23*, 755–764.

(80) Stander, E.; Esterhuysen, C.; McKenzie, J. M.; Cronje, S.; Raubenheimer, H. G. *Dalton Trans.* **2007**, 5684–5691.

(81) Elbjerrami, O.; Yockel, S.; Campana, C. F.; Wilson, A. K.; Omary, M. A. *Organometallics* **2007**, *26*, 2550–2560.

(82) Shi, F.-Q.; Li, X.; Xia, Y.; Zhang, L.; Yu, Z.-X. *J. Am. Chem. Soc.* **2007**, *129*, 15503–15512.

(83) Laitar, D. S.; Müller, P.; Gray, T. G.; Sadighi, J. P. *Organometallics* **2005**, *24*, 4503–4505.

(84) Esswein, A. J.; Dempsey, J. L.; Nocera, D. G. *Inorg. Chem.* **2007**, *46*, 2362–2364.

(85) Mulliken, R. S. *J. Chem. Phys.* **1955**, *23*, 1833–1840.

lengthening and contraction occur in the excited states of auroated naphthalenes and pyrenes.

### Conclusions

Boronic acids and pinacolboronate esters bearing aromatic hydrocarbon substituents arylate gold(I) substrates. Carbon–gold bond formation occurs regiospecifically at the boron-bearing carbon atom. Aromatics having one or two gold(I) centers are readily preparable, and the synthesis protocol applies equally to phosphine or N-heterocyclic carbene co-ligands on gold. The choice of boronated precursors enables gold attachment at ring positions not amenable to electrophilic aromatic substitution, with iridium-catalyzed borylation reactions of hydrocarbons.<sup>42</sup>

Mono- and digold derivatives of naphthalene and pyrene emit primarily through triplet excited states. In some diauroated naphthalenes (having  $C_{2v}$ ) microsymmetry, dual singlet- and triplet-state emission occurs. Luminescence is centered on the polycyclic aromatic hydrocarbon core, as evidenced by structured emission profiles with vibronic spacings characteristic of aromatic ring deformation modes.

Density-functional theory calculations indicate that the frontier orbitals of the parent hydrocarbons are also those of the gold derivatives. Time-dependent DFT calculations reaffirm<sup>8,29</sup> that the carbon–gold  $\sigma$ -bond is nonchromophoric.

The low-energy optical transitions are intraligand in character. Excited-state geometry optimizations indicate minimal ground-state to triplet-state distortions. The prospects for metalated hydrocarbons in designing red- and near-IR emitters are receiving active study.

**Acknowledgment.** The authors thank the National Science Foundation (grant CHE-0749086 to T.G.G.) for support. T.S.T. acknowledges the Fannie and John Hertz Foundation for a predoctoral fellowship; T.G.G. is an Alfred P. Sloan Foundation Fellow. The diffractometer at Case Western Reserve was funded by NSF grant CHE-0541766; that at Youngstown State University, by NSF grant 0087210, by the Ohio Board of Regents grant CAP-491, and by Youngstown State University. We thank E. J. McLaurin for assistance with emission lifetime measurements and Professor D. G. Nocera (Massachusetts Institute of Technology) for access to instrumentation.

**Supporting Information Available:** Thermal ellipsoid projections of crystallographically characterized compounds; optimized Cartesian coordinates of ground-state and triplet **6'**, **7'**, and **16'**; Kohn–Sham orbital energy level diagram for  $C_{2v}$  model compound **7'**. This material is available free of charge via the Internet at <http://pubs.acs.org>.